ACS OMEGA

http://pubs.acs.org/journal/acsodf

Article

Determination of Cocombustion Kinetic Parameters for Bituminous Coal and Pinus Sawdust Blends

Garikai T. Marangwanda,* Daniel M. Madyira, and Chido H. Chihobo

Cite This: *ACS Omega* 2022, 7, 32108−32118

Read Online

ACCESS | Metrics & More | Article Recommendations | Supporting Information

ABSTRACT: Cocombustion of bituminous coal (HC) and Pinus sawdust (PS) was investigated in this paper with the aim of determining the kinetic parameters relevant to cocombustion reactions of their fuel blends. PS was used because it is a waste biomass product capable of generating energy. Motivated by the need to partly substitute HC used in existing boilers with PS, the optimum kinetic parameters at different blending ratios were thus investigated with the ultimate goal of diversifying the energy portfolio for these boilers. Blended samples were prepared with a PS substitution by mass ranging from 0 to 30%, thus producing five samples, namely:100HC, 90HC10PS, 80HC20PS, 70HC30PS, and 100PS. A simultaneous thermogravimetric analyzer was used to investigate the degradation of the fuel samples under a synthetic air atmosphere using 5, 12.5, and 20 °C/min heating rates. The kinetic parameters were evaluated using the distributed activation energy model (DAEM) due to its ability to evaluate complex parallel chemical mechanisms. The influential homogenous volatile combustion and heterogenous combustion stages produced an increasing trend for activation energy (E_a) with increased PS (100HC to 70HC30PS) from an average of 61.80−104.34 kJ/mol while the pre-exponential factor increased from 1.31×10^5 to 6.52×10^8. Generally, blending of HC with PS did not produce a linear variation of the kinetic parameters; thus, by using various plots, an optimum blending ratio of 80HC20PS was deduced.

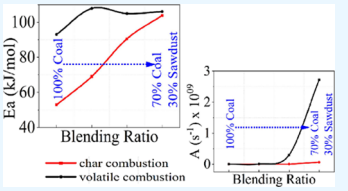

1. INTRODUCTION

Cocombustion of coal and biomass provides an alternative for biomass waste management as well as combustion efficiency improvement for boilers if correctly implemented and monitored during the combustion process.[1] Optimization of cocombustion is necessary since introduction of biomass does not result in a linear variation of thermal parameters but is dependent on a plethora of variables that range from fuel physical and chemical properties to combustion operating conditions.[2,3] Unfortunately, coming up with optimized parameters necessary for the cocombustion process on an experimental basis is expensive and considered confidential by most companies.[4] As such computational fluid dynamics (CFD) offers great potential in terms of addressing the gap related to specific regions not capable of running experimental facilities due to resource constraints. Deliberate policies by developed countries on the use of biomass and coal in some of their existing boilers has already produced some positive feedback.[5] However, since developing countries can now use cost effective CFD, the major hurdle is on the initial boundary conditions which are based on unique experimental data to produce good cocombustion models. Due to the sheer vastness of biomass species, a combination of appropriate modeling and experimental techniques are needed to address the gap that exists with respect to certain species that are employed in the cocombustion process. Since combustion involves chemical reactions, predicting good kinetic parameters forms the basis of good mechanisms that can be used to predict the progression of chemical reactions with improved accuracy.[2]

Combustion of solid fuels is based on the fact that a fuel particle goes through distinct stages when it enters the combustion zone, namely: drying, devolatilization, char combustion, volatile combustion, and ash formation.[6] Drying entails the removal of moisture (surface and inherent) when the particle is heated up to around 105 °C in the absence of oxygen while devolatilization involves removal of light volatiles and heavy volatiles when the heating continues further in the absence of oxygen. The quantitative (mass of volatiles released and the rate of release) and qualitative (chemical composition of volatiles) analysis of volatiles is rather complicated making this stage one of the most important ones in the combustion experimental process. As for CFD, volatile combustion submodels use mechanisms that are mainly based on the results of the devolatilization stage.[7] Char combustion requires knowledge of the reactions that occur within the boundary layer and those occurring within the free stream. Fortunately, the experimental analysis of this stage is less cumbersome when information about the fuel is adequate.[6] However, CFD requires specific input parameters which tend to be overlooked by most of the researchers. Similarly, because of the vast biomass species, it tends to be rather impossible to exhaust all

Received: May 30, 2022
Accepted: July 11, 2022
Published: August 30, 2022

Table 1. Examples of Coal and Biomass Cocombustion Analysis by Use of Thermogravimetry

	experimental method					kinetic method
fuel	biomass blending ratios (% biomass substitution)	max temperature (°C)	heating rate (°C/min)	sample mass (mg)	purge gas	
bituminous coal, lignite, sawdust, rice straw, and catkins[9]	10, 30, 50, 70	900	20	10	air, 80 mL/min	Coats−Redfern
coal and corn stalks biomass[10]	25, 50, 75	850	10, 20, 30, 40, 60	20	80% pure argon and 20% pure nitrogen, 100 mL/min	distributed activation energy model
bituminous coal, corn stalk, and sawdust biomass[11]	10, 20, 30, 50	1000	15, 60	20	air, 100 mL/min	Coats−Redfern
coal and cellulose biomass[1]	25, 50, 75	850	10, 20, 40	10	argon, 60 mL/min	Kissinger−Akahira−Sunose
coal and wood chips[12]	various	1000	10, 20, 30, 40, 50	9	air, 100 mL/min	Flynn−Wall−Ozawa and Kissinger−Akahira−Sunose
coal, biochar, municipal solid waste, and sawdust[13]	various	800	5	7	air, 100 mL/min	Coats−Redfern
coal, torrefied sawdust, paraffin[15]	various	1000	3, 10, 20, 40	10	nitrogen, 100 mL/min	Friedman, Flynn−Wall−Ozawa, and Kissinger−Akahira−Sunose

the possible fuel blend compositions between coal and biomass while testing various operating conditions.[8] As a result, this study is going to produce kinetic parameters for the chosen fuel species that can be later extended to other compatible useful species.

Investigations into cocombustion of coal and biomass have been carried out before on an experimental basis as summarized in Table 1. Guo et al.[9] experiments showed a decreasing trend on the overall activation energy (E_a) as the biomass proportion was increased to about 30% which was also supported by Chen et al.[10] When the biomass proportion was increased beyond 30%, its effect on E_a heavily became dependent on the biomass species under study hence the increasing trend at specific conversion percentages. This is explained by the notion that different temperature ranges are responsible for devolatilization, volatile combustion, and char combustion for biomass vs coal samples. However, from a general perspective, a higher E_a is representative of a lower reactivity as more energy is required to initiate a reaction.[10] To avoid this confusion, Zhou et al.[11] analyzed the E_a representative of the volatile combustion regime separately from the one representative of the char combustion regime. Results showed an increase in E_a as biomass proportion increased from 44.5 to 64.5 kJ/mol for the volatile combustion regime while the E_a representative of the char combustion regime decreased from 94.8 to 35.2 kJ/mol. Even though Mureddu et al.[12] did not investigate coal biomass blends, their findings on individual coal and biomass species suggested Pinus woodchips exhibit better combustion activity than coal. This is evidenced by the E_a difference between bituminous coal and Pinus woodchips corresponding to the volatile combustion regime as well as the char combustion regime. An extensive comparison of the different coal biomass blends for different municipal solid wastes and woody biomass residues was performed by Boumanchar et al.[13] By using the Coats−Redfern[14] (C-R) method, the authors generally found the diffusion and power (nucleation) mechanisms giving the best fit between the model and experimental results. In contrast to other researchers, Florentino-Madiedo et al.[15] showed an increased E_a for both the volatile combustion regime and the char combustion regime, though the synergistic effect was not particularly positive. As such, the complex nature of coal-biomass cocombustion is made apparent by the absence of a generalized trend toward the determination of E_a. Wang et al.[16] performed experiments on coal blended with polyurethane and demonstrated that ignition temperature is inversely proportional to E_a. In as much as different models were employed by the authors to analyze their results, the order of E_a for the coal biomass blends was generally consistent obtaining values between 10 and 200 kJ/mol for the different blending ratios.

Table 2 summarizes some of the industrial applications that have tried to model the cocombustion process of biomass with coal. Generally, the validation of the models (if done) is based on temperature profiles within the furnace which are very sensitive toward kinetic parameters. The general agreement among the reviewed authors is for the need to perform good physical and chemical characterization experiments if the cocombustion models are to improve their accuracy. Most common industrial boilers systems within Zimbabwe utilize bituminous coal as a fuel as mirrored by other boiler systems within the region as well. Eventually, the objective of this study is to facilitate the cocombustion of coal and biomass waste within these boilers. Since sawdust (mainly Pinus) is available as a waste product across the region as well, the researchers saw it worthwhile to select sawdust waste rather than compete for wood. Appropriate disposal of sawdust waste offers a lot of environmental positives.[17,18] After extensive literature research, the authors did not encounter any kinetic triplicate parameters applicable to CFD modeling of Sub-Saharan bituminous coal and Pinus sawdust (PS) blends for the devolatilization, volatile combustion, and char combustion separately as required by good CFD modeling software. This is particularly due to the fact that, apart from lagging behind as a region, most authors overlook how combustion occurs in stages. Though some of the authors have managed to provide the overall kinetic triplicate parameters for the whole combustion process,[19] each stage requires pertinent data to perform successful CFD modeling.

This research will help address the gap that exists with regards to Sub-Saharan coal and biomass cocombustion, thus becoming useful technical data for power plant retrofitting and optimization. To address these gaps, this research focused on investigating the kinetic parameters that are used within the cocombustion of bituminous coal and PS blends by implementing the distributed activation energy model (DAEM).[10]

https://doi.org/10.1021/acsomega.2c03342
ACS Omega 2022, 7, 32108−32118

Table 2. Industrial Applications of Coal and Biomass Cocombustion That Have Been Modeled

	combustion parameters	CFD modeling parameters	
fuel	boiler capacity and type, location, and biomass blending ratios	devolatilization, char combustion, volatile combustion, drag, radiation, and turbulence submodels	observations
pinewood and bituminous coal[22]	1 MW wall-fired pulverized furnace, United Kingdom, 10% by mass biomass substitution	FG-DVC devolatilization, Smith intrinsic char combustion, EDM volatile combustion, Haider and Levenspiel drag, P-1 radiation and, RNG k-ε turbulence submodels	determination of particle diameters and trajectories within the furnace were the main priority they overlooked experiments useful in obtaining kinetic parameters
PS and bituminous coal[5]	150 MW commercial boiler, Chile, 10% by mass biomass substitution, tangential fired pulverized fuel furnace	two competing rates of devolatilization, kinetic/diffusion surface reaction char combustion, EDM volatile combustion, Morsi and Alexander drag, discrete ordinates radiation and, standard and realizable k-ε turbulence submodels	burnout and temperature-related parameters were successfully modeled, most kinetic parameters were generally obtained from the literature
municipal solid waste (sludge) and coal[23]	100 MW commercial boiler, China, 10% by mass biomass max substitution, tangential fired pulverized fuel furnace	single kinetic rate devolatilization, multiple-surface-reaction char combustion, two-step reaction and finite-rate/EDM volatile combustion, P-1 radiation, realizable k-ε turbulence submodels	emphasis was placed on the NO_x emissions obtained coupled with the economic benefits of cocombusting sludge typically obtained generalized parameters from the literature as no specific experiments on sludge characterization were presented
Cynara cardunculus (biomass) and bituminous coal[19]	350 MW commercial boiler, Spain, no substitution, wall-fired pulverized fuel furnace	single rate kinetic devolatilization, single film boundary layer char combustion, mixed-is-reacted volatile combustion, P-1 radiation, standard k-ε turbulence submodels.	focused on gas species distribution within the furnace and burnout parameters performed necessary TGA experiments to obtain kinetic parameters
biomass and lignite[24]	40 kW test facility, Germany, no substitution, vertical pulverized fuel furnace	single rate kinetic devolatilization, multiple-surface-reaction char combustion, Eddy dissipation-concept volatile combustion, discrete ordinate/WSGGM radiation, Reynolds stress model (RSM) turbulence submodels	validated model using velocity profiles acknowledged limitations caused by particle shape and using assumptions for kinetic parameters
wood and coal[25]	500 MW, United Kingdom, no substitution, wall-fired pulverized fuel furnace	FG-DVC devolatilization, multiple-surface-reaction char combustion, Eddy dissipation volatile combustion, Haider and Levenspiel drag, discrete ordinate radiation, realizable k-ε turbulence submodels	temperature-related parameters were successfully modeled generally, most of the boundary conditions were obtained from the literature

https://doi.org/10.1021/acsomega.2c03342
ACS Omega 2022, 7, 32108−32118

2. METHODOLOGY

2.1. Sample Preparation, Proximate, and Elementary Analysis. The bituminous coal used in this research was of thermal grade obtained from Hwange, Zimbabwe, a high exploration region.[20] The sawdust was obtained from local sawmills around the Eastern Highlands which use *Pinus taeda* and *Pinus patula* species as their main timber raw material.[21] The ISO18283:2006 standard was used to prepare the coal and PS samples for further analysis. Grinding of the fuel samples was done using an IKA MF 10 cutting mill and a lab-scale closed ball mill. The samples were then oven-dried at 105 °C for 24 h before being placed on a vibrating shaker for the sieving process. To ensure homogeneity, a particle diameter group between 180 and 250 μm was chosen for subsequent analysis.

The fuel blends were prepared on a mass basis and labeled appropriately with HC representing the bituminous coal and PS representing the Pinus sawdust. The notation that was adopted for the sample labeling hence analysis was, for example, "90HC10PS" representing 90% coal and 10% PS on a mass basis. In total five samples were prepared for further analysis which were: 100HC, 90HC10PS, 80HC20PS, 70HC30PS, and 100PS. A Barnstead Thermolyne 6000 muffle furnace was used to carry out the proximate analysis of the fuel samples. The ISO 562:2010 and ISO 1171:2010 standards were followed throughout the proximate analysis, thus obtaining the volatile matter, ash, and fixed carbon content.[26] Approximately weights of 1 g were used for the proximate analysis, and to ensure result validity, each fuel sample was tested in triplicate. A Thermo Fisher Scientific Flash analyzer (EA 1112) was used to perform the ultimate analysis (CHNS) of the prepared samples using weights of approximately 1.8 mg for each run. The oxygen and fixed carbon content were determined using the difference method.

2.2. Combustion Kinetic Parameter Modeling. The most common experimental method used in conjunction with modeling techniques for combustion kinetic parameter determination is based on finding the mass loss when the sample is under a controlled heating environment. Specifically, this method is referred to as thermogravimetric analysis which requires an instrument capable of capturing the heating temperature range, heating rate, heating atmosphere, and sample mass with accuracy.[27] Basically, the fuel sample degrades within the instrument with α being used to denote the degree of degradation as given by eq 1. M_0 represents the initial weight, M_t represents the sample weight at time t, and M_f represents the final weight over the specific time range.

$$\alpha = \frac{M_0 - M_t}{M_0 - M_f} \tag{1}$$

Thermal degradation being a kinetic process can then be written based on the Arrhenius equation, eq 2, and the rate of thermal degradation, eq 3, to produce a reaction mechanism equation that can be analyzed using experimental data.

$$k(T) = A\cdot\exp\left(-\frac{E}{RT}\right) \tag{2}$$

$$\frac{d\alpha}{dt} = k(T)\cdot f(\alpha) \rightarrow \beta\frac{d\alpha}{dT} = A\cdot\exp\left(-\frac{E_a}{RT}\right)\cdot f(\alpha) \tag{3}$$

where f(α) refers to the reaction mechanism model, $k(T)$ represents the reaction rate constant, A represents the pre-exponential factor (s^{-1}), E_a represents the activation energy (kJ/mol), R represents the universal gas constant (J/mol·K), T represents the temperature (K), and β refers to the heating rate $\beta = dT/dt$ (K/s).[28,29]

Several models have been developed that can be used to link experimental data to combustion reaction mechanisms for kinetic parameter determination. It is important to note that the reaction mechanism model f(α) is unknown at the beginning of any data analysis. Generally, these models used to link experimental data to combustion reaction mechanisms are thus classified as either model fitting methods or isoconversional (model-free) methods.[1] Table 3 summarizes the different models commonly used to analyze experimental data.

Table 3. Model Fitting Methods and Isoconversional Methods

method	description
Coats–Redfern[13,14]	model fitting requires previous knowledge of the reaction mechanism
modified Coats–Redfern[27,30]	isoconversional: an integral method which depends on the temperature integral approximation
Friedman[15]	isoconversional: a differential method that uses determination of the reaction rate at an equivalent stage for various heating rates
Flynn–Wall–Ozawa[15,31]	isoconversional: an integral method which depends on the temperature integral approximation
Vyazovkin[27]	isoconversional: solutions can only be obtained by use of computer algorithms due to complexity and nonlinearity
Kissinger–Akahira–Sunose[15,32]	isoconversional: an integral method which depends on the temperature integral approximation
distributed activation energy[10]	isoconversional: an integral method that acknowledges chemical reactions occurring in parallel

Mathematical integration of eq 3 does not produce an exact solution since integration of $\exp(-E/RT)$ is not exact because of the variables involved. Thus, after rearranging, eq 3 can be rewritten as eq 4. $G(\alpha)$ is used to represent the integrated form of the reaction mechanism model f(α).

$$\int_0^\alpha \frac{d\alpha}{f(\alpha)} = G(\alpha) = \frac{A}{\beta}\cdot\int_0^T \exp\left(-\frac{E}{RT}\right)dT \tag{4}$$

Isoconversional methods are best used when determining kinetic reaction parameters, particularly the E_a without necessarily considering the reaction mechanism model f(α). On the other hand, for model fitting models, eq 4 is integrated to obtain eq 5, though rearranging is still necessary to obtain eq 6.

$$\ln\frac{G(\alpha)}{T^2} = \ln\left[\frac{AR}{\beta E}\left(1 - \frac{2RT}{E}\right)\right] - \frac{E}{RT} \tag{5}$$

$$\ln\frac{G(\alpha)}{T^2} = \ln\left(\frac{AR}{\beta E}\right) - \frac{E}{RT} \tag{6}$$

Fitting experimental data to eq 6 then becomes possible especially after considering certain assumptions. One of these assumptions is that combustion analysis acknowledges that $(1 - 2RT/E) \approx 1$, thus producing a linear equation. As such the experimental data is traced in such a way that $y = \ln[G(\alpha)/T^2]$ is plotted against $x = 1/T$. From a mathematical point of view, the plot of y vs x is supposed to be linear with a gradient of

https://doi.org/10.1021/acsomega.2c03342
ACS Omega 2022, 7, 32108−32118

Table 4. Reaction Model Functions for Combustion[13,16]

reaction model	$G(\alpha)=$	$f(\alpha)=$
reaction order models		
zero order	α	1
first order	$-\ln(1-\alpha)$	$1-\alpha$
nth order (*tested* $n = 2$)	$\frac{1}{n-1}^{*}[(1-\alpha)^{-(n-1)}-1]$	$(1-\alpha)^n$
nucleation models		
power law ($n \neq 1$) (tested $n = 1/2$ and $n = 2$)	$\alpha^{1/n}$	$n\alpha^{(n-1)/n}$
Avrami–Erofeev (tested $n = 1/2$ and $n = 2$)	$[(-\ln(1-\alpha)]^{1/n}$	$n(1-\alpha)[(-\ln(1-\alpha)]^{(n-1)/n}$
geometrical contraction models		
two dimensional (contracting area)	$1-(1-\alpha)^{1/2}$	$2(1-\alpha)^{1/2}$
three dimensional (contracting volume)	$1-(1-\alpha)^{1/3}$	$3(1-\alpha)^{2/3}$
diffusion models		
1D diffusion	α^2	$\frac{1}{2}\alpha$
2D diffusion	$[(1-\alpha)(\ln(1-\alpha)]+\alpha$	$[-\ln(1-\alpha)]^{-1}$
3D diffusion	$[1-(1-\alpha)^{1/3}]^2$	$\frac{3}{2}(1-\alpha)^{2/3}[1-(1-\alpha)^{1/3}]^{-1}$

$-E/R$ and a y-axis intercept of $\ln(AR/\beta E)$.[16] The linear trace is then analyzed to determine the reaction model function with the least error.[28,33] To determine the value of $G(\alpha)$, each reaction model function has a characteristic equation as presented in Table 4.

The method implemented within this study, the DAEM,[10] which is a model-free method, is represented by eq 10. The method is derived from the Kissinger–Akahira–Sunose[15] model, which is an isoconversional model with the only difference between the two being inclusion of the stabilizing constant, 0.6075. The constant 0.6075 is obtained through simplification of eq 9 based on the first order reaction model. Naturally, it means other reaction models from Table 4 are eligible to be employed, but research has proved how a balance between accuracy and complexity is obtained by using the first order reaction mechanism[34]

$$\int_0^{\alpha}\frac{d\alpha}{f(\alpha)}=\frac{A}{\beta}.\int_0^{T}\exp\left(-\frac{E}{RT}\right)dT = \frac{AE}{\beta R}.\int_y^{\infty}\frac{1}{y^2}\exp(-y)dy \tag{7}$$

$$\int_y^{\infty}\frac{1}{y^2}\exp(-y)dy \approx \frac{1}{y^2}\exp(-y) \tag{8}$$

$$\ln\frac{\beta}{T^2}=\ln\left(\frac{AR}{E\int_0^{\alpha}\frac{d\alpha}{f(\alpha)}}\right)-\frac{E}{RT} \tag{9}$$

$$\ln\frac{\beta}{T^2}=\ln\left(\frac{AR}{E}\right)+0.6075-\frac{E}{RT} \tag{10}$$

The DAEM has been known to produce good results especially with complex reactions such as biomass pyrolysis as well as low temperature degradation.[34] The strength of this model is within its ability to acknowledge how parallel reactions occur during the combustion process. Mathematically, plotting of $\ln(\beta/T^2)$ against $1/T$ at a given degree of degradation is supposed to give a linear graph.[35,36] The y-intercept will then be employed to evaluate the pre-exponential factor.

Within this research, goodness of fit was evaluated by calculating the coefficient of determination, R^2, which is a statistical parameter. This is basically a ratio between the total sum of squares of vertical deviations from each data point to the fitted line and the total sum of squares about the mean as given by eq 11.[37] When the value of R^2 was close to 1, it indicated a good fit with regards to the reaction model function chosen.

$$R^2=1-\frac{\sum_{i=1}^{n}(y_i-\hat{y}_i)^2}{\sum_{i=1}^{n}(y_i-\overline{y}_i)^2} \tag{11}$$

2.3. Thermogravimetric Analysis. A Hitachi STA7200RV simultaneous thermogravimetric analyzer was employed as the instrument for the thermogravimetric experimental analysis as represented in Figure 1.

Since the thermal degradation had to resemble combustion, synthetic air was chosen as the purge gas with a constituent by volume of 79% N_2 and 21% O_2. The purge gas flow rate was set at 20 mL/min, which meant under the oxidative environment, excess oxygen was being supplied to assure

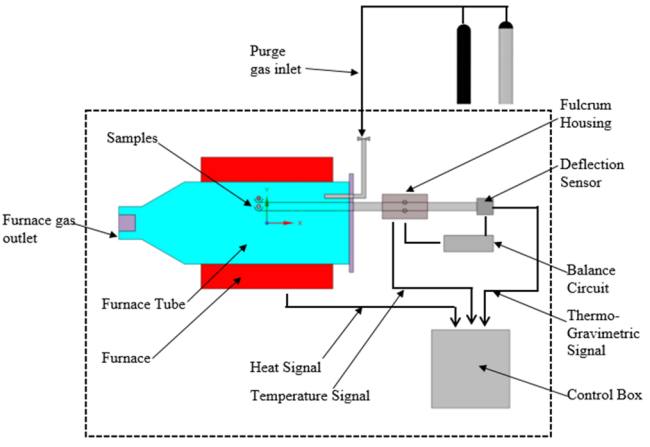

Figure 1. Thermogravimetric analyzer workbench schematic.

https://doi.org/10.1021/acsomega.2c03342
ACS Omega 2022, 7, 32108–32118

Table 5. Chemical Properties of Coal, Pine Sawdust, and Fuel Blends

	proximate analysis[a] (weight %)			ultimate analysis[a] (weight %)				
	fixed carbon[b]	volatile matter	ash	C	H	O[b]	N	S
100HC	53.97	23.10	22.93	58.671	2.946	13.245	1.613	0.593
90HC 10PS	48.21	29.91	21.88	58.489	3.367	14.246	1.448	0.570
80HC 20PS	46.35	31.82	21.83	56.954	3.734	15.632	1.296	0.555
70HC 30PS	46.02	33.74	20.24	56.885	4.093	17.100	1.143	0.535
100PS	15.62	80.68	3.70	49.504	6.035	40.404	0.358	0

[a]On a dry basis. [b]By difference.

complete combustion. The ramp setting was chosen meaning the heating rate could be entered such that the researchers could investigate three heating rates of 5, 12.5, and 20 °C/min. The dynamic temperature range of the instrument was set between 25 and 915 °C meaning no isothermal conditions were investigated. Samples of approximately 10 mg were prepared and fed into an autosampler and a ceramic pan was used for the experiments. The data logger was programmed to record data after every 0.5 s producing the thermogravimetric and differential thermal analysis data automatically. To assure validity of results, some of the fuel samples were tested thrice during the run of the experiments. Data analysis was carried out using Origin Pro 2021 analytical software for better visualization of raw and derived data for further analysis.

3. RESULTS AND DISCUSSION

3.1. Proximate and Ultimate Analysis. Proximate and ultimate analysis results of the fuel samples are summarized in Table 5. The trends relate quite well with previous studies done by other authors showing higher volatile matter for biomass.

The fixed carbon, which is generally higher for coal than biomass, decreases as blending increases, which is the same trend shared for ash. There is no linear variation between the volatile content, ash, and fixed carbon with the blending ratio for the whole range. Generally, substances with high volatile content have a higher ignition tendency while those with high fixed carbon have better combustion stability.[38] Mishra and Mohanty[34] also highlighted how reduced ash content in the fuel/blend results in better combustion properties and reduced fuel preparation costs. Marangwanda et al.[39] further supported the notion by demonstrating how combustion stability decreases as the biomass blending ratio increases due to the increased volatile matter. As noted by Guo et al.,[9] a higher ignition tendency is associated with a lower E_a for the prohomogenous volatile combustion zone, which means the fuel/blend will require less energy to ignite (igniting at lower temperatures).

3.2. Kinetic Parameter Analysis. *3.2.1. TG-DTG Curves of Blended Samples.* Using data obtained from the experiments, TG-DTG curves were traced for the fuel samples under test. The curves have been presented in detail in a previous study by the same authors[39] while a data file also accompanies this publication with all the graphs employed by the authors. The instrument had a sensitivity of 0.1 μg for TG mass readings, which equated to a minimum uncertainty of 0.001% and a maximum value of 0.036% for the values recorded throughout the experiment. Also, since the values were recorded continuously (in case there is some repeated error), it became justifiable to overlook analysis of uncertainty throughout analysis of TG results. An illustrative graph is presented in Figure 2 on how the different points were obtained within this research.

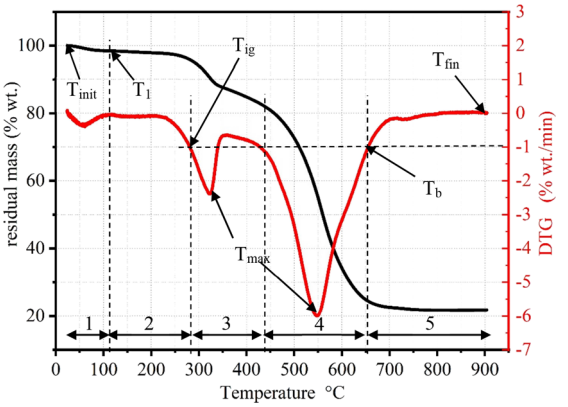

Figure 2. TG-DTG curve for 80HC20PS at a 12.5 °C/min heating rate under an air atmosphere.

As noted by Zhou et al.,[11] thermal degradation of coal makes apparent four stages on the TG-DTG curves which are: low temperature decomposition stage (closely related to inherent moisture release through evaporation), oxygen adsorption stage, homogeneous and heterogeneous combustion stage, and burnout stage. The authors further highlighted that when biomass is blended, the homogenous and heterogenous combustion stage can be split into two distinct stages: the prohomogeneous combustion stage and the proheterogeneous combustion stage. However, they did not manage to determine kinetic parameters for both stages explicitly which this research addressed as well. Within this research, kinetic parameters during the low temperature decomposition were not determined ($T < T_1$). This was supported by the fact that few chemical reactions occurred during this initial stage thus no significant mass loss was experienced.

T_{init} represents the temperature at the start of the experiment thus the release of moisture begins accompanied by a slight decrease in mass. Subsequently, Stage 2 is noted by the region with an almost constant or slight mass increase. This corresponds to the physical and chemical adsorption of the oxygen stage (region between T_1 and T_{ig}). As highlighted by Wang et al.,[16] the reason why the sample mass remains almost constant or increases at first during Stage 2 is because after oxygen adsorption, oxygen-containing complexes are formed on the fuel particle surface. This process is also accompanied by release of light volatiles (decrease in mass) thus a contradicting phenomenon existing during Stage 2. If the release of light volatiles is more significant than the mass gain due to oxygen adsorption, an overall mass loss will be

https://doi.org/10.1021/acsomega.2c03342
ACS Omega 2022, 7, 32108−32118

experienced during Stage 2 thus a decrease of mass in Stage 2 for the 80HC20PS fuel blend.[40]

Of tremendous importance is the point at which ignition occurs symbolized by the region where rapid mass loss commences the TG curves. Within this research, ignition was judged to occur when the mass loss rate was at 1% weight/min as employed by some other authors in their corresponding studies.[27,32] The other method of locating the ignition point which uses tracing of tangents on the TG-DTG curves is too subjective especially when the effect of blending comes into play since some points of inflection became intertwined. The temperature at the ignition point is symbolized by T_{ig}, while the time by t_{ig}. The fuel continued to lose weight until the burnout point when volatile and char combustion were judged to have been completed. The burnout point is also denoted by the point at which the mass loss rate is 1% weight/min after the fuel has lost most of its mass. T_b is used to denote the burnout temperature, while t_b for the time at burnout.

The prohomogeneous volatile and proheterogeneous combustion zones can be made apparent as distinct stages. During the prohomogeneous volatile combustion zone, Stage 3, hydrocarbon active structures on the fuel surface increase exponentially leading to an increased oxygen adsorption and sample degradation rate. The products, tars, volatiles, CO, and CO_2 were then produced in large quantities leading to an increased mass loss rate. Passing into the proheterogeneous combustion zone, volatiles continue to burn while the fixed carbon or char is ignited and combusted. As such, more CO and CO_2 gases are produced leading to an increased mass loss rate.[16] T_{max} is used to show the temperature at which maximum mass loss rate occurs visualized by a peak on the DTG curve, t_{max} the time at that point and DTG_{max} the corresponding mass loss rate. Stages 3 and 4 encompass the most influential reactions related to combustion as most of the mass loss occurs within these regions because of the prohomogeneous and heterogenous combustion reactions. For example, the 80HC20PS sample loses on average 74.6% of its initial weight within this stage. Eventually, as alluded to in the introductory section, the kinetic parameters for each stage were determined exclusively without averaging the parameters for the whole process.[40,41]

3.2.2. Kinetic Analysis by the DAEM. The DAEM method was first used to determine the E_a for the different stages in the combustion process. For a given degree of degradation (α), $\ln(\beta/T^2)$ was traced against $1/T$ to give a linear plot. Using a viable approach proposed by Wang et al.,[32] more emphasis was placed on Stages 3 and 4 with regards to this method. The chosen degrees of degradation of 0.1 up to 0.9 where all within the prohomogeneous and proheterogeneous combustion stage. For example, at a heating rate of 20 °C/min, the prohomogeneous volatile combustion stage began at a degree of degradation of 0.04249 for the 70HC30PS sample, 0.03458 for the 80HC20PS sample, and 0.02843 for the 90HC10PS sample. The proheterogeneous char combustion stage terminated at a degree of degradation of 0.9785 for the 70HC30PS sample, 0.9798 for the 80HC20PS sample, and 0.9821 for the 90HC10PS sample. These lower and upper limits where almost similar for the other heating rates of 12.5 and 5 °C/min. The prohomogeneous combustion stage for the various heating rates had an average degree of degradation upper limit of 0.1877 which led the authors to suggest that the E_a values obtained at degrees of degradation of 0.1 and 0.2 where related to the prohomogeneous combustion stage. The rest of the values where then linked to the proheterogeneous combustion stage.

The values represented in Table 6 were obtained from the plot of $\ln(\beta/T^2)$ against $1/T$ for the samples at 5, 12.5, and 20 °C/min heating rates as shown in Figures 3456. Eq 12 shows the rearranged form that was used to determine the E_a values, while eq 13 shows the corresponding equation used for the pre-exponential factor.

$$E_a\ (\mathrm{kJ/mol}) = \text{gradient} \times [-8.314\ (\mathrm{J/mol\ K})/1000] \tag{12}$$

$$A = \frac{E\ (\mathrm{J/mol})}{R\ (\mathrm{J/mol{\cdot}K})} \times \exp(y - \text{intercept} - 0.6075) \tag{13}$$

The average E_a values for both Stages 3 and 4 were then consolidated as shown in Table 7 for all the fuel samples based on the $\ln(\beta/T^2)$ against $1/T$ plots.

Figure 7 does show that Stage 3 (provolatile combustion) tends to require more energy to activate with regards to blends containing high content of coal. However, the difference between the energy required to activate Stage 3 vs Stage 4 tends to decrease as the blending ratio increases. One possible explanation might be due to the higher energy required to activate the degradation of hemicellulose and cellulose within biomass as postulated by Wnorowska et al.[38] The other explanation might be due to the effect of diffusion within the boundary layer as rightly explained by Sarroza et al.[42] Diffusion of oxygen toward the char particle is hindered by a volatile cloud formed during devolatilization. Consequently, the E_a required to combust a char particle becomes higher whenever high volatile substances are involved. However, it is very important to understand that in a volatile free environment, biomass char is considered more reactive than coal char as investigated by Al-Qayim et al.[43] In agreement, the authors recorded an increase of 43.9% from 72.94 to 104.95 kJ/mol (averaged Stages 3 and 4) in E_a as more PS was introduced.

Figure 8 does demonstrate how E_a varies with degree of conversion for the different fuel samples. Both 100HC and 90HC10PS samples show a clear progression of decreasing E_a as a function of degree of conversion. The 80HC20PS sample then shows a quasi-activation energy between $\alpha = 0.1$ and 0.3, which is then exaggerated by the 70HC30PS sample at $\alpha = 0.2$ with a drop in E_a before increasing and later dropping gradually after $\alpha = 0.4$. Analysis of Figure 2 alongside Figure 8 highlights how the region between $\alpha = 0.1$ and 0.3 falls within the prohomogeneous combustion zone for the 80HC20PS and 70HC30PS samples. As such it makes sense to note that the type of volatiles released from biomass influence combustion progression heavily for any blending greater than the 80HC20PS mass ratio. This can also be seen by the plot in Figure 9, which is generally expected to have a linear gradient to demonstrate a kinetic compensation effect as discussed by Chen et al.[10] Kinetic compensation is generally expected for most heterogenous-based chemical reactions as experienced within this research.[44] As such a compromise between blending ratios and benefits can be obtained from the 80HC20PS sample. Figure 10 compares the behavior of previous studies with the current one with respect to E_a and conversion degree for coal samples. Mureddu et al.[12] during their experiments with bituminous South African coal, which has properties very close to the bituminous coal under test, obtained slightly lower E_a. The average E_a of South African coal was 59.47 kJ/mol while that of the coal under test was 61.80

https://doi.org/10.1021/acsomega.2c03342
ACS Omega 2022, 7, 32108−32118

Table 6. DAEM Method for Fuel Blends Heated in Air at 5, 12.5, and 20 °C/min

	degree of degradation	70HC30PS			80HC20PS			90HC10PS			100HC		
		R^2	E (kJ/mol)	A (s^{-1})	R^2	E (kJ/mol)	A (s^{-1})	R^2	E (kJ/mol)	A (s^{-1})	R^2	E (kJ/mol)	A (s^{-1})
Stage 3	α = 0.1	0.9980	113.02	5.358×10^{9}	0.9980	105.99	5.64×10^{8}	0.9980	214.89	6.51×10^{16}	0.9980	100.35	1.12×10^{6}
	α = 0.2	0.9965	99.09	7.832×10^{7}	0.9965	103.90	2.48×10^{7}	0.9965	107.89	5.05×10^{6}	0.9965	85.61	4.71×10^{4}
Stage 4	α = 0.3	0.9988	117.06	3.361×10^{8}	0.9988	106.74	4.86×10^{6}	0.9988	92.15	1.61×10^{5}	0.9988	75.86	6.56×10^{3}
	α = 0.4	0.9963	121.62	8.355×10^{7}	0.9963	104.36	1.35×10^{6}	0.9963	83.76	2.67×10^{4}	0.9963	66.90	1.20×10^{3}
	α = 0.5	0.9910	113.66	7.333×10^{6}	0.9910	99.08	3.46×10^{5}	0.9910	75.94	5.72×10^{3}	0.9910	58.45	2.53×10^{2}
	α = 0.6	0.9818	105.19	9.792×10^{5}	0.9818	92.81	9.06×10^{4}	0.9818	67.87	1.28×10^{3}	0.9818	50.14	5.65×10^{1}
	α = 0.7	0.9675	98.27	2.158×10^{5}	0.9675	83.79	1.68×10^{4}	0.9675	60.04	3.04×10^{2}	0.9675	43.58	1.67×10
	α = 0.8	0.9540	90.04	4.215×10^{4}	0.9540	77.08	4.43×10^{3}	0.9540	54.20	9.66×10	0.9540	39.13	6.84×10^{0}
	α = 0.9	0.9602	81.09	6.713×10^{3}	0.9602	69.79	9.87×10^{2}	0.9602	48.97	3.24×10	0.9602	36.21	3.48×10^{0}
			104.34	6.52×10^{8}		93.73	6.62×10^{7}		73.85	6.56×10^{5}		61.80	1.31×10^{5}

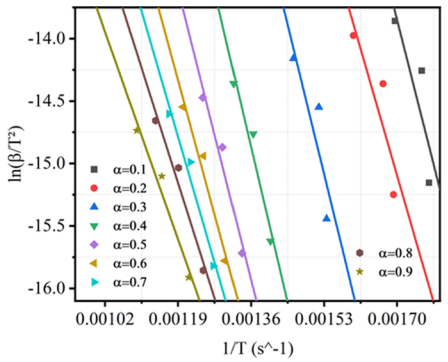

Figure 3. Plot of $\ln[\beta/T^2]$ vs $1/T$ for 70HC30PS at 5, 12.5, and 20 °C/min under an air atmosphere.

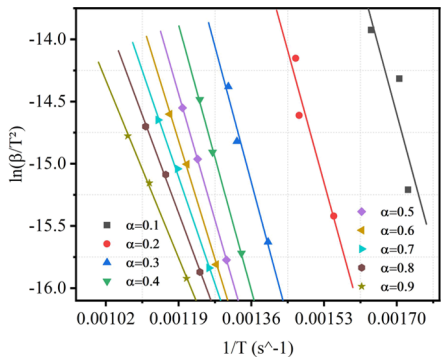

Figure 4. Plot of $\ln[\beta/T^2]$ vs $1/T$ for 80HC20PS at 5, 12.5, and 20 °C/min under an air atmosphere.

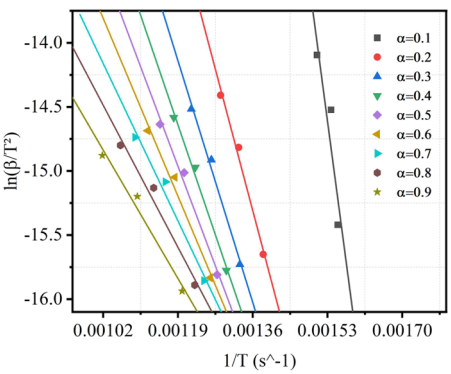

Figure 5. Plot of $\ln[\beta/T^2]$ vs $1/T$ for 90HC10PS at 5, 12.5, and 20 °C/min under an air atmosphere.

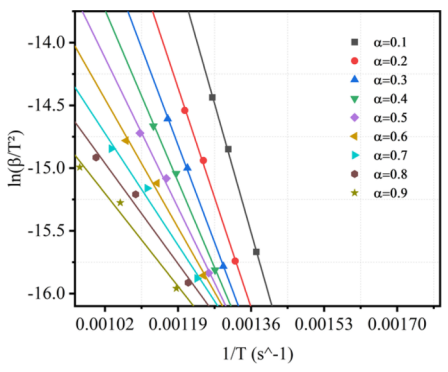

Figure 6. Plot of $\ln[\beta/T^2]$ vs $1/T$ for 100HC at 5, 12.5, and 20 °C/min under an air atmosphere.

https://doi.org/10.1021/acsomega.2c03342
ACS Omega 2022, 7, 32108−32118

Table 7. DAEM Activation Energy and Pre-Exponential Factor Values for the Fuel Blends Heated in Air

fuel blend	stage	E (kJ/mol)	A (s^{-1})
100HC	Stage 3	92.98	5.84×10^5
	Stage 4	52.90	1.16×10^3
90HC10PS	Stage 3	107.89	5.05×10^6
	Stage 4	68.99	2.78×10^4
80HC20PS	Stage 3	104.95	2.94×10^8
	Stage 4	90.52	9.53×10^5
70HC30PS	Stage 3	106.05	2.718×10^9
	Stage 4	103.85	6.118×10^7

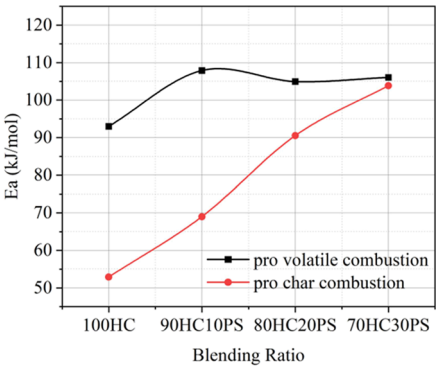

Figure 7. Plot of E_a vs blending ratio.

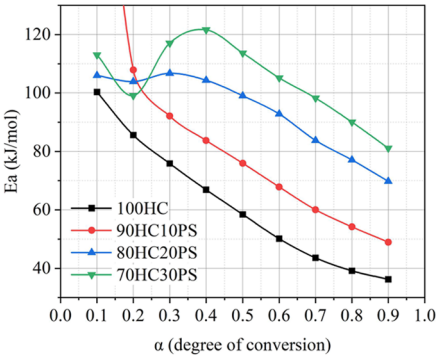

Figure 8. Plot of E_a vs degree of conversion.

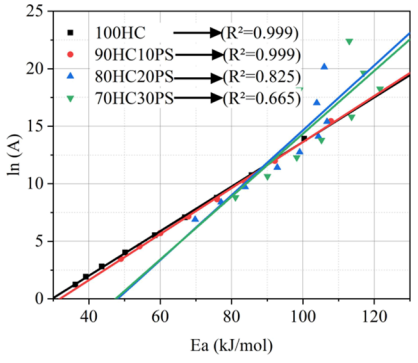

Figure 9. Plot of ln(A) vs activation energy.

kJ/mol. The slight difference might be due to the heating rates employed by Mureddu et al.[12] (10, 20, 30, 40, and 50 °C/min heating rates) as well as the modeling method used, Kissinger–Akahira–Sunose (KAS). However, as supported by other authors that used the KAS method with respect to coal, the E_a associated with Stages 3 and 4 is around 80–150 kJ/mol while that associated with biomass is around 60–193 kJ/mol.[31,35,36] Wang et al.[27] also demonstrated how coal containing blends have an E_a between 85 and 143 kJ/mol with regards to the combined Stages 3 and 4.

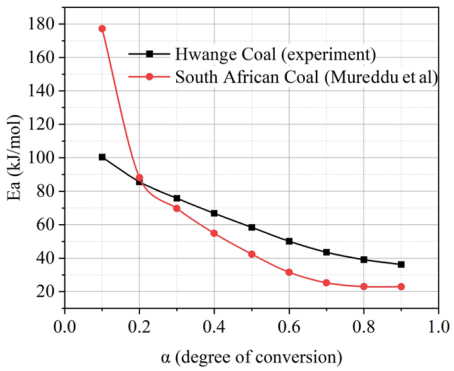

Figure 10. Plot of activation energy comparison vs degree of conversion of Hwange coal and South African coal.

4. CONCLUSIONS

Through experimental work coupled with modeling techniques, the kinetic parameters of HC and PS blends were determined with success. The research gap existent due to the need of having correct combustion parameters necessary for optimum operation of most boilers that are moving toward greener energy was addressed within this research. Experimental work was necessary so as to generate boundary conditions that can be used for further optimization of combustion boilers. This was mainly because no linear relation could be deduced that could link sample blending proportions to expected kinetic parameters. In conclusion:

The higher volatile composition within PS was responsible for a decrease in ignition temperature from 457.70 to 265.76 °C as the mass proportion was increased from 0 to 30% for a heating rate of 20 °C/min. The biochar obtained from PS was deduced to have catalyzed the decrease in burnout temperature as well by 14.64% from 820.05 to 699.97 °C. The DTG curve developed two peaks as soon as PS was blended with the first peak being linked to homogenous volatile combustion while the second peak was linked to heterogenous char combustion.

The kinetic parameters that were evaluated using the DAEM produced no linear trends as the PS proportion was increased from 0 to 30%. The influential homogenous volatile combustion produced an increasing trend for activation energy (E_a) with an increased PS mass ratio (100HCto 70HC30PS) from 92.98 to 106.05 kJ/mol. The heterogeneous combustion stage also produced an increasing trend from 52.90 to 103.85 kJ/mol. Similarly, the pre-exponential factor increased with blending for both homogenous and heterogenous combustion from 5.84×10^5 to 2.72×10^9 s^{-1} and 1.16×10^3 to 6.12×10^7 s^{-1}, respectively.

Good kinetic compensation is obtained for the 100HC and 90HC10PS samples guiding the authors to suggest an optimum blending ratio of 80HC20PS when all the appropriate parameters are taken into account. This blending ratio guaranteed a large change in E_a which symbolized maximum influence of PS at reduced blending ratios. This is particularly important for cofiring facilities that do not need to change most of their operating conditions when they cater for biomass substitution.

https://doi.org/10.1021/acsomega.2c03342
ACS Omega 2022, 7, 32108–32118

In summary, the necessary boundary conditions related to cocombustion of HC and PS blends were evaluated at different blending ratios resulting in parameters for each combustion stage, namely, devolatilization, volatile combustion, and char combustion.

■ ASSOCIATED CONTENT

Supporting Information

The Supporting Information is available free of charge at https://pubs.acs.org/doi/10.1021/acsomega.2c03342.

> $\ln[\beta/T^2]$ vs $1/T$ for 100HC, 90HC10PS, 80HC20PS, and 70HC30PS at 5, 12.5, and 20 °C/min under an air atmosphere (Figures S1−S4);TG and DTG for 100HC, 90HC10PS, 80HC20PS, and 70HC30PS at 5, 12.5, and 20 °C/min under an air atmosphere (Figures S5−S18); TG and DTG synergistic coefficients for 90HC10PS, 80HC20PS, and 70HC30PS at 5, 12.5, and 20 °C/min under an air atmosphere (Figures S19 and S20); E_a vs blending ratio/degree of conversion (Figures S21−S24); and ignition index with heating rate/combustion indexes/pre-exponential vs blending ratio (Figures S25−S27) (PDF)

■ AUTHOR INFORMATION

Corresponding Author

Garikai T. Marangwanda − *Department of Mechanical Engineering Science, University of Johannesburg, Johannesburg 2006, South Africa; Department of Fuels and Energy Engineering, School of Engineering Sciences and Technologies, Chinhoyi University of Technology, Chinhoyi, Zimbabwe;* orcid.org/0000-0002-3746-957X; Phone: +27-620-259-829; Email: gmarangwanda@gmail.com

Authors

Daniel M. Madyira − *Department of Mechanical Engineering Science, University of Johannesburg, Johannesburg 2006, South Africa*

Chido H. Chihobo − *Department of Fuels and Energy Engineering, School of Engineering Sciences and Technologies, Chinhoyi University of Technology, Chinhoyi, Zimbabwe*

Complete contact information is available at: https://pubs.acs.org/10.1021/acsomega.2c03342

Author Contributions

G. M. was responsible for conceptualization, formal analysis, investigation, methodology, and writing of the manuscript. D. M. was responsible for funding acquisition, resources as well as reviewing and editing of the manuscript. C. C. helped with the methodology as well as manuscript reviewing and editing. All authors have read and agreed to the published version of the manuscript.

Notes

The authors declare no competing financial interest.

■ ACKNOWLEDGMENTS

The authors specially thank both the University of Johannesburg, South Africa, and Chinhoyi University of Technology, Zimbabwe, for supporting them during this research.

■ NOMENCLATURE

Units

E_a	activation energy (kJ/mol)
T	static temperature (K)
m	mass (g)
Qv	volume flow rate (mL/min)
$k(T)$	reaction rate constant
A	pre-exponential factor (s^{-1})
t	time (s)
R	universal gas constant (J/mol·K)
C	synergistic effect coefficient
R^2	coefficient of confidence

Abbreviations

HC	bituminous coal
PS	Pinus sawdust
TGA	thermogravimetric analysis
CR	Coats−Redfern
KAS	Kissinger-Akahira−Sunose
CFD	computational fluid dynamics
FG-DVC	functional group depolymerization volatile cross-linking
EDM	Eddy dissipation model
RNG	renormalization group
WSGGM	weighted sum of gray gases model
RSM	Reynolds stress model
DTG	TG first derivative
DSC	differential scanning calorimetry curve

Subscripts

0 or in	initial weight
t	weight at time t
max	maximum
i	species
exp	experimental
f or fin	final weight
ig	ignition

Greek Symbols

k	turbulence kinetic energy ($m^2\ s^{-2}$)
α	degree of degradation
β	heating rate (K/s)
ϵ	dissipation rate of k ($m^2\ s^{-3}$)

■ REFERENCES

(1) Wu, Z.; Zhang, J.; Zhang, B.; Guo, W.; Yang, G.; Yang, B. Synergistic Effects from Co-Pyrolysis of Lignocellulosic Biomass Main Component with Low-Rank Coal: Online and Offline Analysis on Products Distribution and Kinetic Characteristics. *Appl. Energy* **2020**, *276*, No. 115461.

(2) Liu, Q.; Zhong, W.; Tang, R.; Yu, H.; Gu, J.; Zhou, G.; Yu, A. Experimental Tests on Co-Firing Coal and Biomass Waste Fuels in a Fluidised Bed under Oxy-Fuel Combustion. *Fuel* **2021**, *286*, No. 119312.

(3) Tang, R.; Liu, Q.; Zhong, W.; Lian, G.; Yu, H. Experimental Study of SO 2 Emission and Sulfur Conversion Characteristics of Pressurized Oxy-Fuel Co-Combustion of Coal and Biomass. *Energy Fuels* **2020**, *34*, 16693−16704.

(4) Sankar, G.; Kumar, D. S.; Balasubramanian, K. R. Computational Modeling of Pulverized Coal Fired Boilers − A Review on the Current Position. *Fuel* **2019**, *236*, 643−665.

(5) Pérez-Jeldres, R. R.; Cornejo, P.; Flores, M.; Gordon, A.; García, X. A Modeling Approach to Co-Firing Biomass/Coal Blends in Pulverized Coal Utility Boilers: Synergistic Effects and Emissions Profiles. *Energy* **2017**, *120*, 663−674.

(6) Turns, S. *An Introduction to Combustion: Concepts and Applications*, 2nd ed.; McGraw-Hill series in mechanical engineering; McGraw-Hill: New York, 1996.
(7) Marangwanda, G. T.; Madyira, D. M.; Babarinde, T. O. Coal Combustion Models: A Review. In *International Conference on Engineering for Sustainable World*; Institute of Physics Publishing, 2019; Vol. *1378*, pp. 1−11.
(8) Álvarez, A.; Pizarro, C.; García, R.; Bueno, J. L.; Lavín, A. G. Determination of Kinetic Parameters for Biomass Combustion. *Bioresour. Technol.* **2016**, *216*, 36−43.
(9) Guo, F.; He, Y.; Hassanpour, A.; Gardy, J.; Zhong, Z. Thermogravimetric Analysis on the Co-Combustion of Biomass Pellets with Lignite and Bituminous Coal. *Energy* **2020**, *197*, No. 117147.
(10) Chen, X.; Liu, L.; Zhang, L.; Zhao, Y.; Zhang, Z.; Xie, X.; Qiu, P.; Chen, G.; Pei, J. Thermogravimetric Analysis and Kinetics of the Co-Pyrolysis of Coal Blends with Corn Stalks. *Thermochim. Acta* **2018**, *659*, 59−65.
(11) Zhou, C.; Liu, G.; Wang, X.; Qi, C. Co-Combustion of Bituminous Coal and Biomass Fuel Blends: Thermochemical Characterization, Potential Utilization and Environmental Advantage. *Bioresour. Technol.* **2016**, *218*, 418−427.
(12) Mureddu, M.; Dessì, F.; Orsini, A.; Ferrara, F.; Pettinau, A. Air- and Oxygen-Blown Characterization of Coal and Biomass by Thermogravimetric Analysis. *Fuel* **2018**, *212*, 626−637.
(13) Boumanchar, I.; Chhiti, Y.; M'hamdi Alaoui, F. E.; Elkhouakhi, M.; Sahibed-dine, A.; Bentiss, F.; Jama, C.; Bensitel, M. Investigation of (Co)-Combustion Kinetics of Biomass, Coal and Municipal Solid Wastes. *Waste Manage.* **2019**, *97*, 10−18.
(14) Coats, A. W.; Redfern, J. P. Kinetic Parameters from Thermogravimetric Data. *Nature* **1964**, *201*, 68−69.
(15) Florentino-Madiedo, L.; Vega, M. F.; Barriocanal, C. Evaluation of Synergy during Co-Pyrolysis of Torrefied Sawdust, Coal and Paraffin. A Kinetic and Thermodynamic Study. *Fuel* **2021**, *292*, No. 120305.
(16) Wang, H.; Tian, Y.; Li, J.; Chen, X. Experimental Study on Thermal Effect and Gas Release Laws of Coal-Polyurethane Cooperative Spontaneous Combustion. *Sci. Rep.* **2021**, *11*, 1994.
(17) IEA. *World Energy Outlook 2017*; International Energy Agency: Paris, France, 2017; pp. 1−15.
(18) Bloomberg New Energy Finance. The Clean Energy Country Competitiveness Index. *Clim.* **2016**, *2016*, 91.
(19) Pallarés, J.; Herce, C.; Gil, A.; Cortés, C.; Herce, C. Numerical Study of Co-Firing Coal and Cynara Cardunculus in a 350 MWe Utility Boiler. *Fuel Process. Technol.* **2009**, *90*, 1207−1213.
(20) Hancox, P. J. The Coalfields of South-Central Africa: A Current Perspective. *Episodes* **2016**, *39*, 407−428.
(21) Hyde, M.; Wursten, B.; Ballings, P.; Palgrave Coates, M. Flora of Zimbabwe: Species information: Pinus patula. Flora of Zimbabwe. https://www.zimbabweflora.co.zw/speciesdata/species.php?species_id=102970 (accessed 2021-05-26).
(22) Ma, L.; Gharebaghi, M.; Porter, R.; Pourkashanian, M.; Jones, J. M.; Williams, A. Modelling Methods for Co-Fired Pulverised Fuel Furnaces. *Fuel* **2009**, *88*, 2448−2454.
(23) Tan, P.; Ma, L.; Xia, J.; Fang, Q.; Zhang, C.; Chen, G. Co-Firing Sludge in a Pulverized Coal-Fired Utility Boiler: Combustion Characteristics and Economic Impacts. *Energy* **2017**, *119*, 392−399.
(24) Benim, A. C.; Deniz Canal, C.; Boke, Y. E. Computational Investigation of Oxy-Combustion of Pulverized Coal and Biomass in a Swirl Burner. *Energy* **2022**, *238*, No. 121852.
(25) Black, S.; Szuhánszki, J.; Pranzitelli, A.; Ma, L.; Stanger, P. J.; Ingham, D. B.; Pourkashanian, M. Effects of Firing Coal and Biomass under Oxy-Fuel Conditions in a Power Plant Boiler Using CFD Modelling. *Fuel* **2013**, *113*, 780−786.
(26) Zhu, Q. *Coal Sampling and Analysis Standards*; IEA Clean Coal Centre: London, 2014.
(27) Wang, C.; Liu, Y.; Zhang, X.; Che, D. A Study on Coal Properties and Combustion Characteristics of Blended Coals in Northwestern China. *Energy Fuels* **2011**, *25*, 3634−3645.
(28) Niu, S. L.; Lu, C. M.; Han, K. H.; Zhao, J. L. Thermogravimetric Analysis of Combustion Characteristics and Kinetic Parameters of Pulverized Coals in Oxy-Fuel Atmosphere. *J. Therm. Anal. Calorim.* **2009**, *98*, 267−274.
(29) Li, H.; Niu, S.; Lu, C.; Wang, Y. Comprehensive Investigation of the Thermal Degradation Characteristics of Biodiesel and Its Feedstock Oil through TGA−FTIR. *Energy Fuels* **2015**, *29*, 5145−5153.
(30) Dhaundiyal, A.; Singh, S. B.; Hanon, M. M.; Rawat, R. Determination of Kinetic Parameters for the Thermal Decomposition of Parthenium Hysterophorus. *Environ. Clim. Technol.* **2018**, *22*, 5−21.
(31) Niu, S.; Chen, M.; Li, Y.; Song, J. Co-Combustion Characteristics of Municipal Sewage Sludge and Bituminous Coal. *J. Therm. Anal. Calorim.* **2018**, *131*, 1821−1834.
(32) Wang, C.; Zhang, Y.; Wang, P.; Zhang, J.; Du, Y.; Che, D. Effects of Silicoaluminate Oxide and Coal Blending on Combustion Behaviors and Kinetics of Zhundong Coal under Oxy-Fuel Condition. *J. Therm. Anal. Calorim.* **2018**, *134*, 1975−1986.
(33) Chen, P.; Zhang, L.; Huang, K. Kinetic Modeling of Coal Thermal Decomposition under Air Atmosphere. *Energy Fuels* **2016**, *30*, 5158−5166.
(34) Mishra, R. K.; Mohanty, K. Pyrolysis Kinetics and Thermal Behavior of Waste Sawdust Biomass Using Thermogravimetric Analysis. *Bioresour. Technol.* **2018**, *251*, 63−74.
(35) Ren, L. F.; Li, Q. W.; Deng, J.; Yang, X.; Ma, L.; Wang, W. F. Inhibiting Effect of CO2 on the Oxidative Combustion Thermodynamics of Coal. *RSC Adv.* **2019**, *9*, 41126−41134.
(36) Kongkaew, N.; Pruksakit, W.; Patumsawad, S. *Thermogravimetric Kinetic Analysis of the Pyrolysis of Rice Straw*; Elsevier B.V., 2015; Vol. *79*.
(37) OriginLab Cooperation. *Origin Pro*; OriginLab Cooperation: Northampton, 2021.
(38) Wnorowska, J.; Ciukaj, S.; Kalisz, S. Thermogravimetric Analysis of Solid Biofuels with Additive under Air Atmosphere. *Energies* **2021**, *14*, 2257.
(39) Marangwanda, G. T.; Madyira, D. M.; Ndungu, P. G.; Chihobo, C. H. Combustion Characterisation of Bituminous Coal and Pinus Sawdust Blends by Use of Thermo-Gravimetric Analysis. *Energies* **2021**, *14*, 7547.
(40) Lü, H. F.; Deng, J.; Li, D. J.; Xu, F.; Xiao, Y.; Shu, C. M. Effect of Oxidation Temperature and Oxygen Concentration on Macro Characteristics of Pre-Oxidised Coal Spontaneous Combustion Process. *Energy* **2021**, *227*, No. 120431.
(41) Seifali Abbas-Abadi, M.; Fathi, M.; Ghadiri, M. Effect of Different Process Parameters on the Pyrolysis of Iranian Oak Using a Fixed Bed Reactor and TGA Instrument. *Energy Fuels* **2019**, *33*, 11226−11234.
(42) Sarroza, A. C.; Bennet, T. D.; Eastwick, C.; Liu, H. Characterising Pulverised Fuel Ignition in a Visual Drop Tube Furnace by Use of a High-Speed Imaging Technique. *Fuel Process. Technol.* **2017**, *157*, 1−11.
(43) Al-Qayim, K.; Nimmo, W.; Hughes, K.; Pourkashanian, M. Kinetic Parameters of the Intrinsic Reactivity of Woody Biomass and Coal Chars via Thermogravimetric Analysis. *Fuel* **2017**, *210*, 811.
(44) Barrie, P. J. The Mathematical Origins of the Kinetic Compensation Effect: 1. the Effect of Random Experimental Errors. *Phys. Chem. Chem. Phys.* **2012**, *14*, 318−326.

https://doi.org/10.1021/acsomega.2c03342
ACS Omega 2022, 7, 32108−32118